




 Cite this: *RSC Adv.*, 2022, **12**, 27596

# Femtosecond coherent anti-Stokes Raman spectroscopy study of vibrational dynamics of liquid chloroform

 Honglin Wu,  Yunfei Song, YangYang Zeng, Gangbei Zhu, Guoyang Yu\* and Yanqiang Yang \*

Femtosecond time-resolved coherent anti-Stokes Raman spectroscopy (CARS) was used to study the dynamics of the vibrational modes of liquid chloroform. The vibrational modes were selectively excited and their coherent vibrational dynamics were obtained. Some subtle features that are difficult to distinguish in the ordinary spontaneous Raman spectrum, such as overtones and combinations of some fundamental vibrational modes, were recognized from the CARS transients. Combined with theoretical calculations, the contributions of chlorine isotopes were also confirmed from the CARS transients of the vibrational modes involving the motion of chlorine atoms.

 Received 22nd July 2022  
 Accepted 7th September 2022

DOI: 10.1039/d2ra04542g

[rsc.li/rsc-advances](http://rsc.li/rsc-advances)

## 1. Introduction

Time-resolved coherent anti-Stokes Raman spectroscopy (tr-CARS) has been widely used to study molecular vibrational dynamics. In tr-CARS, a Raman-active vibrational mode is coherently excited when the energy difference between the simultaneous incident pump and Stokes pulse is tuned to be resonant with the transition of this vibrational mode. The coherently excited vibration is probed by the probe pulse, and the generated anti-Stokes Raman signal is emitted in the phase-matching direction. By scanning the delay time between the probe pulse and the pump/Stokes pulses, coherent vibrational dynamics can be obtained. W. Kiefer and co-workers have carried out a lot of pioneering work in this field.<sup>1–4</sup> They demonstrated the application of femtosecond tr-CARS to study the vibrational dynamics of the electronic ground or excited states of gas- and liquid-phase materials. V. A. Apkarian *et al.* also carried out a lot of research on vibrational dynamics using femtosecond tr-CARS, in particular the vibrational dynamics of I<sub>2</sub> molecules in solids at low temperature.<sup>5–7</sup> Using tr-CARS, this group then reported the first real-time record of vibrational wave packet motion at the single-molecule limit.<sup>8</sup> Vibrational dynamics obtained by CARS can help understand the reaction mechanisms in various materials, such as energetic materials.<sup>9–11</sup> In addition to the studies of vibrational dynamics, CARS can also be used for imaging and diagnostics. As a kind of label-free imaging technology, CARS microscopy has been widely used in biology and medicine.<sup>12–15</sup> The CARS transient of nitrogen molecules can be used to measure temperature in

reacting flows.<sup>16,17</sup> These remarkable works indicate that CARS is an effective tool for studying the microscopic mechanism of chemical reactions both in organisms and inorganic materials.

When femtosecond laser pulses are used as pump and Stokes, Raman-active vibrational modes in the range of hundreds of wavenumbers can be excited. If two or more vibrational modes are excited simultaneously, polarization beats will be observed in the CARS transients when probed by femtosecond pulses.<sup>1,18–21</sup> Using femtosecond tr-CARS, spectral information can be obtained not only directly from the frequency domain, but also through the analysis of polarization beats, which may have higher precision. With the advances in laser and photodetector technology, femtosecond CARS has achieved higher detection sensitivity and can provide more and more detailed characteristics of vibration dynamics in experiments.

Chloroform is a common organic solvent with the fewest atoms in a single molecule and consequently the fewest normal vibrational modes. It is often chosen as a sample to study the vibration-related processes and the interactions with other molecules. In the early work, the vibrational relaxation of chloroform molecules was obtained by analyzing the Raman line shape.<sup>22–24</sup> In the room-temperature condensed-phase system, the line shape of the spectrum is modified by a variety of homogeneous and inhomogeneous broadening, so it is difficult to access accuracy dynamics parameters from Raman spectra. As a time-domain approach to vibration, CARS was used in some work to get the dephasing time constants of some specific vibrational modes, such as C–H stretching vibration.<sup>25,26</sup> In our previous work, the vibrational dynamics of the CH stretching vibration of chloroform was studied by multiplex CARS.<sup>27</sup> Although different modes were simultaneously excited, the application of white-light continuum

National Key Laboratory of Shock Wave and Detonation Physics, Institute of Fluid Physics, China Academy of Engineering Physics, Mianyang, China. E-mail: yuguoyang@caep.cn; yqyang@caep.cn



greatly reduced the intensity of the CARS signal, resulting in large errors in extracting the information of a single mode. To our knowledge, there is little work on the systematic study of the vibrational dynamics of chloroform by direct time-domain detection methods. In this paper, the vibrational dynamics of liquid chloroform was systematically investigated using femto-second CARS with higher sensitivity. The CARS transients of all the vibrational modes were obtained at room temperature. Compared with the previous results, the signal-to-noise ratio of the CARS curves was greatly improved. Besides the more reliable dynamics derived from the high quality experimental data, many subtle features that are difficult to distinguish in spontaneous Raman spectra were also observed.

## 2. Experimental

The schematic diagram of the CARS experimental setup is shown in Fig. 1(A). The output laser beam (802 nm, 100 fs, 1 kHz) from a Ti:sapphire regenerative amplifier (Spitfire Ace, Spectra Physics) was divided into two beams by a 9 : 1 beam splitter. The laser beam with 90% energy was used to pump an optical parametric amplifier (OPA) (TOPAS, Light Conversion). The wavelength-tunable laser beam output from the OPA was further divided by a 1 : 1 beam splitter into two beams, which were used as the pump and probe, respectively. The 802 nm laser beam with 10% energy was used as the Stokes beam. The timing of the pump, Stokes and probe laser pulses was adjusted by their respective optical delay lines. The delay time between the pump pulse and the Stokes pulse was adjusted to zero to ensure that they interact with the sample simultaneously, and the delay time between the probe pulse and the other two laser pulses was scanned to get the CARS transient. The three laser beams (after appropriate attenuation) were then focused into the sample in the folded BOXCARS geometry by a lens with a focal length of 300 mm, as shown in Fig. 1(B). The generated

CARS signal is naturally separated from the incident laser beams, and can be spatially selected and then directed into a micro optical fiber spectrometer (QE Pro, Ocean Insight). In the tr-CARS experiments in this work, the center wavelength of the Stokes pulses was fixed at 802 nm, and the center wavelength of the pump/probe pulses was tuned by adjusting the OPA to realize the selective excitation of specific vibrational modes. As shown in Fig. 1(C), when the energy difference between the pump pulse and the Stokes pulse is resonant with a certain vibrational mode, this mode will be selectively excited and detected. By scanning the wavelength of the pump laser, all the Raman-active modes can be selectively excited one by one, and their vibrational dynamics can then be obtained. For all the vibrational modes, the laser power of the pump, Stokes and probe beams was all 0.1 mW in the CARS experiments.

The spontaneous Raman spectrum of chloroform was obtained by a home-built experimental setup, in which a 532 nm single longitudinal mode CW laser (Samba, Cobolt) was used as the excitation source. The excitation laser was focused on the sample through a 10× microscopic objective, and the light power arriving at the sample was about 0.13 mW. A spectrometer with a focal length of 500 mm and a grating of 1800 grooves/mm (SR-500i, Andor) combined with a charge-coupled device (CCD) (DR-316B, Andor) was used to detect the Raman spectrum. The acquired spectrum was calibrated with the standard Raman spectrum of naphthalene. The sample in this work was liquid chloroform (purity  $\geq 99\%$ ), which was placed in a quartz cuvette with an optical path of 1 mm without further purification. All the experiments were carried out at room temperature.

## 3. Results and discussion

### 3.1 Normal vibrational modes of chloroform

The chloroform molecule has highly symmetrical geometry that belongs to the  $C_{3v}$  point group. A chloroform molecule has 5

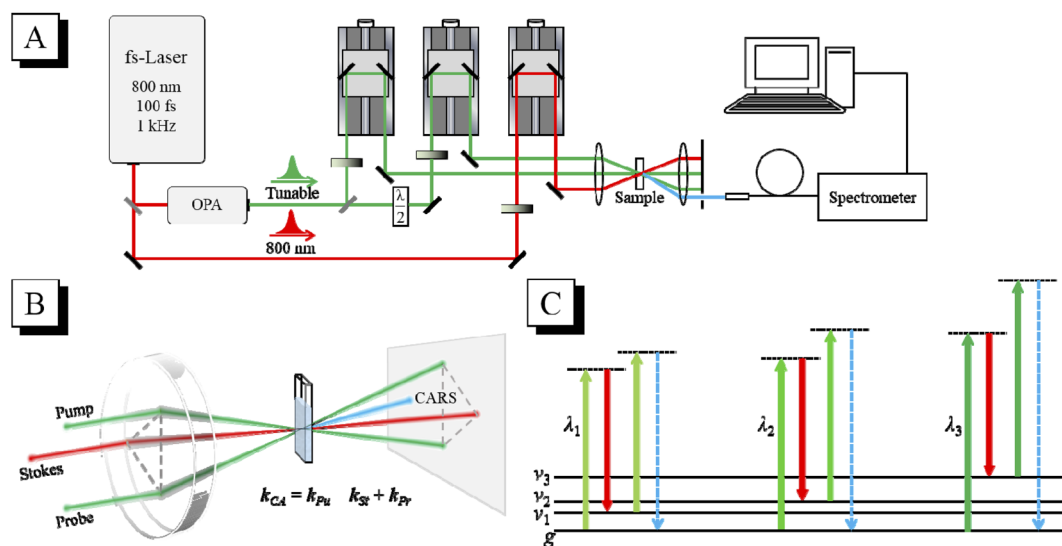


Fig. 1 (A) Schematic diagram of the fs-CARS experimental setup. (B) Folded BOXCARS geometry of the three incident laser beams. The generated CARS signal is spatially separated from the incident laser beams. (C) Schematic of selective excitation. The wavelength of the pump pulse is tuned to selectively excite each vibrational mode.



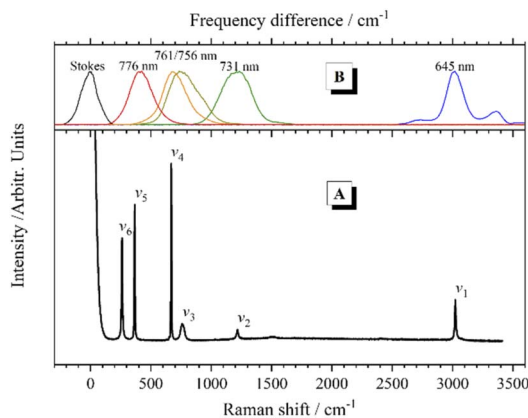


Fig. 2 (A) Spontaneous Raman spectrum of chloroform at room temperature. (B) Spectra of the Stokes pulse (black line) and the selected pump/probe pulses (colored lines), with frequency difference relative to the Stokes pulse as horizontal coordinate.

atoms and consequent 9 normal vibrational modes, all of which are Raman active. The normal vibrational modes of chloroform were calculated at the B3LYP/6-311++G(d,p) level using Gaussian 03.<sup>28</sup> According to the calculation results, 3 pairs of normal vibrational modes are degenerate or have almost identical vibrational energy, so only 6 Raman bands contributed by the fundamental modes can be observed in the Raman spectrum, as shown in Fig. 2(A). The experimental and calculated frequencies of these vibrational modes and their assignments are listed in Table 1.

In the CARS experiments, the center wavelength of the Stokes pulse was kept unchanged at 802 nm, while the output of the OPA was tuned to 645 nm, 731 nm, 756 nm, 761 nm and 776 nm to selectively excite the corresponding vibrational modes of chloroform molecules, respectively. Fig. 2(B) shows the frequency differences between these pump pulses and the 802 nm Stokes pulse, which match the Raman peaks in the spontaneous Raman spectrum. It should be mentioned that, since the bandwidth (full width at half maximum; FWHM) of the femtosecond laser pulses is about  $300\text{ cm}^{-1}$ , the width of the effective excitation band generated by the pump and the Stokes pulses may exceed  $600\text{ cm}^{-1}$ . Therefore, only the CH stretching mode can be excited separately. When the other vibrational modes are desired to be excited, multiple vibrational

Table 1 Vibrations of chloroform

Mode	Vibrational frequency ( $\text{cm}^{-1}$ )		Assignment
	Experimental	Calculated	
$\nu_1$	3023	3181.56	CH stretching
$\nu_2$	1218	1245.25/1245.25	CH $d^a$ -bending
$\nu_3$	761	729.41/729.39	CCl <sub>3</sub> $d$ -stretching
$\nu_4$	669	661.73	CCl <sub>3</sub> $s^b$ -stretching
$\nu_5$	367	364.74	CCl <sub>3</sub> $s$ -deformation
$\nu_6$	261	261.19/261.18	CCl <sub>3</sub> $d$ -deformation

<sup>a</sup>  $d$  here stands for degenerate. <sup>b</sup>  $s$  here stands for symmetric.

modes within the excitation bandwidth will be excited simultaneously, and obvious polarization beats will emerge in the time domain CARS transient. Besides, considering the output laser pulse with a wavelength near 802 nm from the OPA was not that stable, the direct selective excitation of  $\nu_6$  mode with the pump pulse at 784 nm was cancelled. When  $\nu_5$  was excited with the pump pulse at 776 nm,  $\nu_6$  was also in the effective excitation range. Then the dynamics of  $\nu_6$  can be obtained by analyzing the polarization beats generated between them.

### 3.2 Vibrational dynamics of chloroform

In order to analyze the vibrational dynamics, it is necessary to fit the experimental transient curves to obtain the desired parameters. The following formula is usually used to describe the change of CARS signal intensity with delay time:<sup>20</sup>

$$I_{\text{as}}(t) \propto \left| \sum_j A_j \exp(-t/\tau_j) \exp[-i(\omega_j t - \phi_j)] \right|^2. \quad (1)$$

Here,  $I_{\text{as}}(t)$  is the time-dependent intensity of the CARS signal, and  $t$  is the delay time.  $A_j$  represents the pre-exponential factor of the  $j^{\text{th}}$  mode, and  $\tau_j$ ,  $\omega_j$ ,  $\phi_j$  are the dephasing time, angular frequency, and initial phase of the  $j^{\text{th}}$  mode, respectively. Not only the coherent dynamics of a single vibrational mode, but also the coherent dynamics of multiple vibrational modes that are simultaneously excited can be described by eqn (1).

**3.2.1.  $\nu_1$  mode (CH stretching).** Fig. 3 shows the experimental result of selective excitation of  $\nu_1$ . It can be seen from the inserted contour map that the CARS signal appears at around 540 nm, as the wavelength of the pump/probe pulse was tuned to 645 nm. (A 600 nm short-pass edge filter was used to filter out the scattered light of the pump/probe.) In CARS experiments, the time when the probe pulse temporally coincides with the pump/Stokes pulse is usually defined as the time zero. A main component of the signal occurs at time zero is the nonresonant background that arises from the response of electrons to the electric field of the incident laser pulses. The signal intensity of

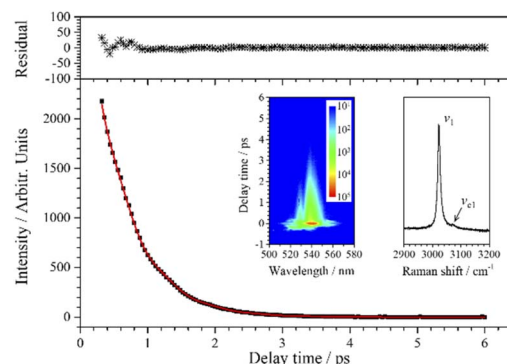


Fig. 3 CARS transient of  $\nu_1$  at 540 nm. The red line is the single exponential fit to the experimental data (black squares). The upper subgraph shows the fitting residuals. The inserted contour map (left) shows the two-dimensional CARS signal around 540 nm, and the other inserted graph (right) shows the partially enlarged Raman spectrum for  $\nu_1$ .



the nonresonant background is usually higher than that of the molecular vibrations, and they can even differ by several orders of magnitude in fs-CARS experiments. Nevertheless, because of the ultrafast response of electrons, the duration of the nonresonant background is basically the same as the convolution of the probe and pump/Stokes pulses. Compared with the dephasing of the vibrational modes, the lifetime of the nonresonant background from electrons is usually much shorter, and the skipping of the nonresonant background has little effect on the analysis of the vibrational dynamics. Thus, only the CARS transients at positive delay times that mainly contributed by the vibrational modes are considered in the following analysis.

Since the CH stretching mode  $\nu_1$  ( $3023\text{ cm}^{-1}$ ) appears as a single peak in the spontaneous Raman spectrum, the decay of the CARS signal of  $\nu_1$  should be an ideal single exponential decay in principle. However, when the experimental data are fitted with a single exponential decay function, there is a weak periodic oscillation emerged in the residuals. That is, some other component contributes to this CARS transient. When two components are considered ( $j = 2$ ) in the fitting process, the fitted curve (red) obtained by eqn (1) is in good agreement with the experimental data (black squares), and the beat frequency (*i.e.* the angular frequency difference between two vibrations) is fitted to be  $49\text{ cm}^{-1}$  (to facilitate analysis, the fitted beat frequency is directly given in wavenumbers here and in the following analysis). It means that, besides  $\nu_1$ , there is another component contributing to the oscillation signal with a pre-exponential factor ratio of 0.018 to  $\nu_1$ , and the frequency difference between them is  $49\text{ cm}^{-1}$ .

When the spontaneous Raman spectrum around  $3000\text{ cm}^{-1}$  is partially enlarged, shown as an insert in Fig. 3, a weak shoulder can be distinguished at  $3072\text{ cm}^{-1}$ , labeled as  $\nu_{c1}$ . The frequency difference between  $\nu_1$  ( $3023\text{ cm}^{-1}$ ) and  $\nu_{c1}$  is just coincident with beat frequency appearing in the CARS transient. Although the intensity of  $\nu_{c1}$  itself is very weak, the high intensity  $\nu_1$  can be regarded as a local oscillation, and their cross term forms a relatively more obvious oscillation in the CARS transient. Therefore, the parameters of the dynamics of  $\nu_{c1}$  can be easily obtained by analyzing the polarization beats. The fitting result shows that the dephasing time constants of  $\nu_{c1}$  and  $\nu_1$  are both about 1.11 ps. Even though the Raman spectrum of chloroform was obtained nearly a hundred years ago, there is no definite assignment about this Raman peak at about  $3072\text{ cm}^{-1}$ . The first reporter of this peak believed that the peak was from the residual aliphatic or aromatic impurities in chloroform,<sup>29</sup> and some other researchers assigned it to the  $2\nu_5 + 3\nu_3$  combination, which appeared due to Fermi resonance mixing with  $\nu_1$ .<sup>30</sup> The almost identical dephasing time constants of  $\nu_1$  and  $\nu_{c1}$  obtained in this experiment also suggests a possible coupling between the two vibrational modes. We suggest that  $\nu_{c1}$  may most likely originate from the third overtone of  $\nu_3$  ( $4\nu_3$ ), which may be easier to access since the first overtone can directly be observed in the Raman spectrum.

**3.2.2.  $\nu_2$  mode (CH stretching).**  $\nu_2$  is the normal mode with the lowest oscillation strength. The CARS signal intensity of  $\nu_2$  is much lower than that of the nonresonant background. In order

to get a transient curve with a good signal-to-noise ratio (SNR), the exposure time of the detector needs to be increased. Under the circumstance, the nonresonant background signal will saturate the detector. So the acquisition of the CARS transient of  $\nu_2$  was started from the delay time of 0.5 ps to avoid the influence of the nonresonant background.

As shown in the inserted contour map in Fig. 4, the CARS signal of  $\nu_2$  appears at around 671 nm when the pump/probe light is centered at 731 nm. (A 700 nm short-pass edge filter was used to filter out the scattered light of the pump/probe.) In this inserted contour map with intensity depicted on a logarithmic scale, there is another vibrational signal appearing at around 697 nm (the signal above 700 nm was blocked by a short-pass filter) with lower intensity and longer lifetime. This signal is assigned to  $\nu_4$  which is covered by the effective excitation range formed by the pump and Stokes pulses, even though the efficiency is very low. The beat pattern appears (around 685 nm in the inserted contour map in Fig. 4) between the two vibrational signals with a frequency fitted to  $550\text{ cm}^{-1}$  is also evidence for the participation of  $\nu_4$ . Compared with  $\nu_4$ ,  $\nu_3$  is too weak to be distinguished in the CARS signal under this excitation condition.

The weak-intensity oscillation in the CARS transient curve indicates the coherence between  $\nu_2$  and other vibrational modes. The experimental data are also well fitted when  $j = 2$  using eqn (1) and the fitted beat frequency is  $120\text{ cm}^{-1}$ . The pre-exponential factor ratio of the weak component to the strong component is 0.034. When the spontaneous Raman spectrum around  $\nu_2$  is partially enlarged, shown as the insert in Fig. 4, a very weak peak can be vaguely distinguished at about  $1339\text{ cm}^{-1}$ , which is labeled as  $\nu_{c2}$ .  $\nu_{c2}$  may also come from the overtones or combination of some low-frequency normal modes, most possibly the first overtone of  $\nu_4$ . It is worth noting that unlike the case of  $\nu_{c1}$  and  $\nu_1$ , there may be no coupling between  $\nu_{c2}$  and  $\nu_2$ , since there is a certain difference between the fitted dephasing time constants of  $\nu_{c2}$  (0.8 ps) and  $\nu_2$  (0.69 ps).

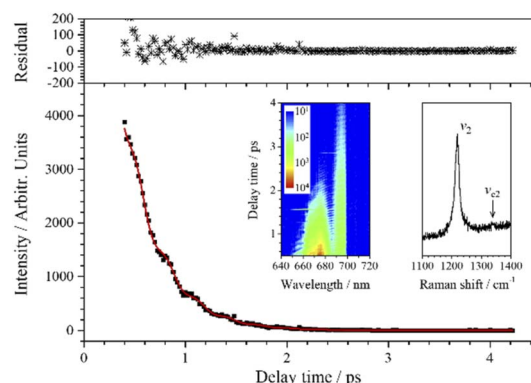


Fig. 4 CARS transient of  $\nu_2$  at 671 nm. The red line is the fit to the experimental data (black squares) when two vibrational modes are involved. The upper subgraph shows the fitting residuals. The inserted contour map (left) shows the two-dimensional CARS signal around 671 nm, and the other inserted graph (right) shows the partially enlarged Raman spectrum for  $\nu_2$ .

**3.2.3.  $\nu_3$  mode (degenerate  $\text{CCl}_3$  stretching).** In the low-frequency vibration region of chloroform, the intervals between different vibrations are small, so it is impossible to directly excite a specific vibrational mode with femtosecond laser pulses without affecting the nearby vibrations. When the pump/probe pulse was tuned to 756 nm, the  $\nu_3$  mode is excited with the highest efficiency, and correspondingly the CARS signal of  $\nu_3$  appears at 715 nm. (A 750 nm short-pass edge filter was used to filter out the scattered light of the pump/probe.) At the same time, the nearby  $\nu_4$  mode will also be efficiently excited, and the edge of the effective excitation range even covers the  $\nu_5$  mode. The CARS signal of  $\nu_4$  appears at 720 nm under this excitation condition, as shown in the insert contour map in Fig. 5. Since the frequency difference between  $\nu_3$  and  $\nu_4$  is  $92\text{ cm}^{-1}$ , polarization beats of  $92\text{ cm}^{-1}$  can be expected. As the Raman intensity of  $\nu_4$  is much stronger than that of  $\nu_3$ ,  $\nu_4$  is the main component even in the transient curve at 715 nm, and then the short-lived oscillation indicates a fast dephasing of  $\nu_3$ . Although  $\nu_5$  is excited under this condition, it has little effect on the signal at 715 nm, while it contributes to the high-frequency polarization beats with a frequency of  $302\text{ cm}^{-1}$  around 730 nm (as shown in the inserted contour map in Fig. 5) due to its coherence with  $\nu_4$ .

The experimental transient curve at 715 nm is well fitted when  $j$  is taken 3, and the fitting result is shown in Fig. 5. This means that the transient consists of three main components. Although  $\nu_3$  is not the dominant component in the transient, reliable dynamic parameters of  $\nu_3$  can still be obtained from the fitting process. Besides  $\nu_3$ , there are two other vibrational modes (with a wavenumber interval of about  $4.5\text{ cm}^{-1}$ ) participating in the polarization beats at 715 nm, and their assignment will be discussed below.

**3.2.4.  $\nu_4$  mode (symmetric  $\text{CCl}_3$  stretching).** In order to excite the  $\nu_4$  mode most effectively, the center wavelength of the pump/probe pulse was tuned to 761 nm, and correspondingly the CARS signal of  $\nu_4$  is centered at about 724 nm. (A 750 nm short-pass edge filter was used to filter out the scattered light of the pump/probe.) In this case, although  $\nu_3$  can also be effectively

excited, its intensity is much lower than that of  $\nu_4$ . While, since  $\nu_5$  is at the edge of the effective excitation band, its excitation efficiency is not that high. Thus,  $\nu_3$  and  $\nu_5$  have little effect on the CARS transient at 724 nm, but contribute to the polarization beats at both wings of the signal spectrum, respectively.

Although the experimental curve of  $\nu_4$  seems to exhibit a single exponential decay, the experimental data cannot be fitted by a single exponential decay function. Instead, when two vibrational components are involved in the fitting process ( $j = 2$ ), the experimental data are well fitted by the red fitting curve, as shown in Fig. 6. It indicates that there are indeed polarization beats in the experimental curve, and the fitted beat frequency is about  $4.5\text{ cm}^{-1}$ . This splitting may originate from the isotopes of chlorine. However, because the beat period is too long relative to the dephasing of  $\nu_4$ , the decay curve cannot even cover a complete period, the fitting results are unreliable and unable to reflect the real polarization beats. As for contribution of chlorine isotopes to the CARS signal, the following analysis of  $\nu_5$  will give more reliable results.

In addition, it needs to be explained that the relatively large residuals below 3 ps are not due to the low SNR, but because there is still a weak high-frequency beat pattern from the coherence between  $\nu_4$  and  $\nu_5$  at 724 nm. The beat amplitude is very small, thus the influence is not considered in the fitting process, which leads to the relatively large residuals.

**3.2.5.  $\nu_5$  mode (symmetric  $\text{CCl}_3$  deformation).** For the Raman shift of the  $\nu_5$  mode, the corresponding pump wavelength should be centered at 779 nm. However, in the experiment, the pump/probe pulse was tuned to 776 nm to ensure the stability of the OPA output. The corresponding CARS signal appears at around 755 nm, as shown in the inserted contour map in Fig. 7. In this case,  $\nu_4$  and  $\nu_6$  can also be effectively excited, and their corresponding CARS signals appear at around 738 nm and 761 nm, respectively.  $\nu_4$  and  $\nu_6$  are coherent with  $\nu_5$ , producing polarization beats with frequencies of  $302\text{ cm}^{-1}$  and  $106\text{ cm}^{-1}$ , respectively. The polarization beats with a frequency of  $106\text{ cm}^{-1}$  appear within the first 5 ps. The time scale shown in Fig. 7 is relatively long, so that the  $106\text{ cm}^{-1}$  polarization beats are not obvious in the contour map. The  $302\text{ cm}^{-1}$

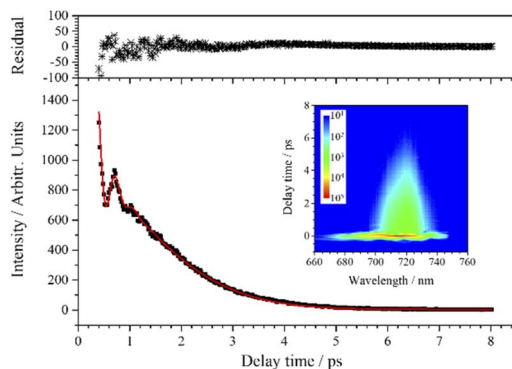


Fig. 5 CARS transient of  $\nu_3$  at 715 nm. The red line is the fit to the experimental data (black squares) when three components are considered. The upper subgraph shows the fitting residuals. The inserted contour map shows the two-dimensional CARS signal around 715 nm.

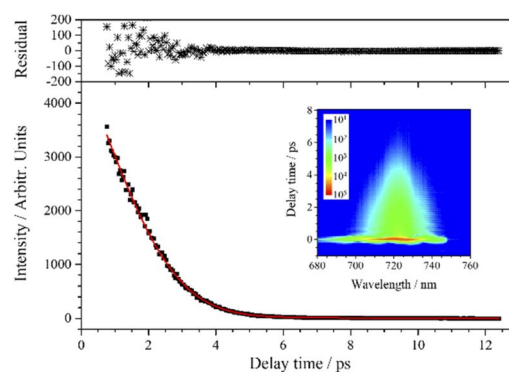


Fig. 6 CARS transient of  $\nu_4$  at 724 nm. The red line is the fit to the experimental data (black squares) when two components are involved. The upper subgraph shows the fitting residuals. The inserted contour map shows the two-dimensional CARS signal around 724 nm.



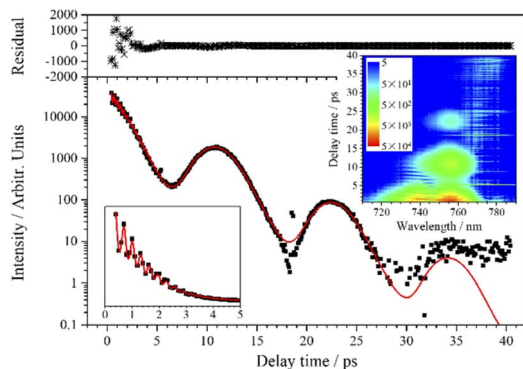


Fig. 7 CARS transient of  $\nu_5$  at 755 nm. The red line is the fit to the experimental data (black squares) when five components are involved. The upper subgraph shows the fitting residuals. The lower left corner shows the zooming out within 5 ps, and the inserted contour map shows the two-dimensional CARS signal around 755 nm.

polarization beats show obvious frequency distortion in this experimental result due to undersampling, because the delay step in the experiment of  $\nu_5$  was 100 fs, corresponding to a sampling frequency of 10 THz, which is shorter than twice the signal frequency.

Similar to the transient of the  $\nu_4$  mode, there is also a low-frequency polarization beat pattern in the transient of  $\nu_5$ . The  $\nu_5$  mode shows the longest dephasing time, and three oscillation periods can be distinguished in the experimental curve, so a more reliable analysis of the low-frequency polarization beats is allowed. As the decay of the signal spans several orders of magnitude, in order to exhibit the oscillation characteristics more clearly, the signal curve of  $\nu_5$  is plotted on a logarithmic scale, as shown in Fig. 7. The transient of  $\nu_5$  is also fitted by eqn (1). When five components are involved ( $j = 5$ ), the experimental curve is well fitted, as shown in Fig. 7.

From the beats with a frequency of  $106 \text{ cm}^{-1}$  within the first 5 ps, it can be determined that  $\nu_6$  is one of the five participating components. The other four components have very close vibrational frequencies, which possibly come from the different combinations of chlorine isotopes. It is known that chlorine has two major isotopes,  $^{35}\text{Cl}$  and  $^{37}\text{Cl}$ , with natural abundances of 75.77% and 24.23%, respectively. Since the  $^{37}\text{Cl}$  atom is heavier than the  $^{35}\text{Cl}$  atom, a vibrational mode involving  $^{37}\text{Cl}$  has lower frequency than the same mode involving  $^{35}\text{Cl}$ . Taking into

account these two isotopes, chloroform molecules have four possible combinations ( $\text{CH}^{35}\text{Cl}_3$ ,  $\text{CH}^{35}\text{Cl}_2^{37}\text{Cl}$ ,  $\text{CH}^{35}\text{Cl}^{37}\text{Cl}_2$ ,  $\text{CH}^{37}\text{Cl}_3$ ), and their proportions and the corresponding calculated vibrational frequencies of  $\nu_5$  are listed in Table 2. For comparison, the fitting parameters of the four components corresponding to the four combinations of chlorine isotopes are also listed in this table. Comparing the parameters listed in Table 2, the relative proportions of  $A_j$  are very close to the calculated proportions of the four combinations. The frequency differences between the fitted frequencies are basically consistent with the calculated frequency differences as well, and they are in good agreement with the fine structure measured under high dispersion.<sup>31</sup> Therefore, it can be confirmed that the low-frequency polarization beats in the CARS transient of  $\nu_5$  originate from the coherence between the symmetric  $\text{CCl}_3$  deformation vibrations with different combinations of chlorine isotopes.

**3.2.6.  $\nu_6$  mode (degenerate  $\text{CCl}_3$  deformation).** The excitation and detection conditions of the  $\nu_6$  mode were basically the same as those of  $\nu_5$ , except that the scanning step of probe was adjusted to 20 fs, for the dephasing time of  $\nu_6$  is much shorter than that of  $\nu_5$ . Under these conditions,  $\nu_4$ ,  $\nu_5$  and  $\nu_6$  can all be effectively excited, as shown in the insert contour map in Fig. 8. With such a time resolution, the polarization beats of  $302 \text{ cm}^{-1}$  formed by  $\nu_4$  and  $\nu_5$  can be correctly distinguished, and polarization beats of  $106 \text{ cm}^{-1}$  formed by  $\nu_5$  and  $\nu_6$  can be depicted more clearly.

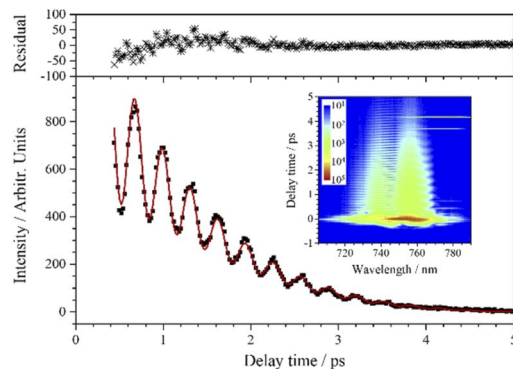


Fig. 8 CARS transient of  $\nu_6$  at 761 nm. The red line is the fit to the experimental data (black squares) when three components are involved. The upper subgraph shows the fitting residuals. The inserted contour map shows the two-dimensional CARS signal around 761 nm.

Table 2 Upper sub-table: calculated proportions of chloroform molecules with different combinations of chlorine isotopes and the corresponding vibrational frequencies of  $\nu_5$ . Lower sub-table: fitting parameters using eqn (1) when  $j = 5$  (the parameters belonging to  $\nu_6$  mode are not listed)

	$\text{CH}^{35}\text{Cl}_3$	$\text{CH}^{35}\text{Cl}_2^{37}\text{Cl}$	$\text{CH}^{35}\text{Cl}^{37}\text{Cl}_2$	$\text{CH}^{37}\text{Cl}_3$
Calculated Proportion (%)	43.50	41.73	13.35	1.42
Frequency of $\nu_5$ ( $\text{cm}^{-1}$ )	364.74	361.93	359.05	356.10
Fitting parameters when $j = 5$				
$A_j$ (relative proportion in %)	86 (46.5)	72 (38.9)	23 (12.4)	4 (2.2)
$\omega_j$ ( $\text{cm}^{-1}$ )	370.85	368.00	365.15	362.30



**Table 3** Vibrational components involved in the CARS transients at the selected signal wavelengths and the corresponding fitted dephasing times

Mode	Signal wavelength <sup>a</sup> (nm)	Participating component <sup>b</sup>	Dephasing time (ps)
$\nu_1$	540	$\nu_1, \nu_{c1}$	$1.110 \pm 0.002, 1.105 \pm 0.002$
$\nu_2$	671	$\nu_2, \nu_{c2}$	$0.692 \pm 0.003, 0.802 \pm 0.003$
$\nu_3$	715	$\nu_3, \nu_4$	$0.22 \pm 0.01, 2.5 \pm 0.1^c$
$\nu_4$	724	$\nu_4^d$	$2.5 \pm 0.1^d$
$\nu_5$	755	$\nu_5^e, \nu_6$	$7.6 \pm 0.2^e, 1.28 \pm 0.05$
$\nu_6$	761	$\nu_5^f, \nu_6$	$7.6 \pm 0.2^f, 1.28 \pm 0.05$

<sup>a</sup> Signal wavelengths where the transient curves are selected to extract the vibrational dynamics. <sup>b</sup> The vibrational components that contribute to the beat patterns in the transient signals. <sup>c</sup> The dephasing time of  $\nu_4$  obtained by fitting the transient at 715 nm is covered in the probable range of that obtained by fitting the transient at 724 nm, so the latter is listed here. <sup>d</sup> Two  $\nu_4$  modes with different chlorine isotopic combinations are involved to obtain a good fit. Their dephasing times are very close, and the mean value is listed here. <sup>e</sup> Four  $\nu_5$  modes with different chlorine isotopic combinations are considered to participate in the CARS transient, and the mean value is listed. <sup>f</sup> Only two chlorine isotopic combinations of  $\nu_5$  modes are considered in the fit of the transient, and their mean value is listed.

The CARS signal corresponding to  $\nu_6$  appears at around 761 nm, and the experimental curve is shown in Fig. 8. The oscillation feature mainly comes from the coherence between  $\nu_5$  and  $\nu_6$ . Taking into account the chlorine isotopes,  $j$  should be taken 5 in the fitting, but the dephasing time of  $\nu_6$  is relatively short, and the low-frequency oscillation feature introduced by chlorine isotopes cannot be effectively revealed in such a short time scale. In this case, it is not necessary to introduce too many components into the fitting process, as is the case with  $\nu_4$ . As a component with relatively low intensity,  $\nu_6$  contributes more to the frequency and the amplitude decay of the polarization beats, so reducing the number of types of  $\nu_5$  will not directly affect the accuracy of the fitting parameters of  $\nu_6$ . As shown in Fig. 8, the experimental data are well fitted when  $j = 3$ , except that the residuals deviate a little from the zero line, which maybe result from insufficient consideration of all the combinations. It is worth noting that the fitting curve well reproduces the oscillation feature in the experimental curve, which means that the fitting parameters belonging to  $\nu_6$  are reliable.

It can be noticed that the effects of carbon and hydrogen isotopes are not observed in the present work, because the natural abundances of  $^{13}\text{C}$  and D are 1.11% and 0.016%, respectively, which are much smaller than that of  $^{37}\text{Cl}$ .

### 3.3 The dephasing times of chloroform vibrational modes

In the above analysis, the transient curves of all the normal vibrational modes are fitted. The fitted dephasing times at room temperature are summarized and listed in Table 3. It is necessary to give some interpretations on the dephasing times. First, two different chlorine isotopic combinations of  $\nu_4$  are involved in the fit at 724 nm and their fitted dephasing times are very close, so the mean value is listed in Table 3. Second, since the mass difference between different chlorine isotopes is small, the dephasing time differences between the different isotopic combinations of the same vibrational mode are very small, the dephasing time of  $\nu_5$  is fixed in the fit processes performed at 755 nm and 761 nm in order to reduce the number of variables. Third,  $\nu_4, \nu_5$  and  $\nu_6$  participate in the transients at different selected wavelengths, their dephasing times given in Table 3 are the mean of the values obtained at different wavelengths.

## 4. Conclusions

Highly sensitive fs-CARS was used to systematically study the vibration of chloroform, and the transients of all the normal vibrational modes at room temperature are detected and analyzed. By fitting the high-quality CARS transients, not only precise dephasing times were obtained, but also some subtle features that were difficult to distinguish in spontaneous Raman spectra were recognized, including the overtones and combinations of some normal vibrational modes, and the vibrational energy splitting induced by chlorine isotopes. The weak subtle features do modulate the CARS transients and their intensities are enhanced by the heterodyne effect in the coupling between adjacent vibrational modes, which makes the subtle features have higher possibility to be extracted from the time-domain CARS signals. Although the complexity will increase for complex molecules under the excitation and probe with femto-second laser pulses, femtosecond time-resolved CARS has the potential to provide subtle spectra of the species in chemical reactions and may help determine the reaction pathways.

## Conflicts of interest

There are no conflicts to declare.

## Acknowledgements

Funding for this work was provided by the National Natural Science Foundation of China (Grant No. 21903075) and National Science and Technology Major Project (Grant No. 2017-III-0005-0030).

## References

- M. Schmitt, G. Knopp, A. Materny and W. Kiefer, *J. Phys. Chem. A*, 1998, **102**, 4059–4065.
- T. Chen, A. Vierheilg, P. Waltner, W. Kiefer and A. Materny, *Chem. Phys. Lett.*, 2000, **325**, 176–182.
- T. Chen, A. Vierheilg, W. Kiefer and A. Materny, *Phys. Chem. Chem. Phys.*, 2001, **3**, 5408–5415.



- 4 G. Yu, Y. Zeng, W. Guo, H. Wu, G. Zhu, Z. Zheng, X. Zheng, Y. Song and Y. Yang, *J. Phys. Chem. A*, 2017, **121**, 2565–2571.
- 5 M. Karavitis, R. Zadoyan and V. A. Apkarian, *J. Chem. Phys.*, 2001, **114**, 4131–4140.
- 6 M. Karavitis, T. Kumada, I. U. Goldschleger and V. A. Apkarian, *Phys. Chem. Chem. Phys.*, 2005, **7**, 791–796.
- 7 V. Senekerimyan, I. Goldschleger and V. A. Apkarian, *J. Chem. Phys.*, 2007, **127**, 214511.
- 8 S. Yampolsky, D. A. Fishman, S. Dey, E. Hulkko and V. A. Apkarian, *Nat. Photonics*, 2014, **8**, 650–656.
- 9 J. Franken, S. A. Hambir and D. D. Dlott, *AIP Conf. Proc.*, 1998, **429**, 819–822.
- 10 G. Yu, Y. Zeng, W. Guo, H. Wu, G. Zhu, Z. Zheng, X. Zheng, Y. Song and Y. Yang, *J. Phys. Chem. A*, 2017, **121**, 2565–2571.
- 11 N. K. Katturi, S. Dev G, N. Kommu, G. K. Podagatlapalli and V. R. Soma, *Chem. Phys. Lett.*, 2020, **756**, 137843.
- 12 A. Zumbusch, G. R. Holtom and X. S. Xie, *Phys. Rev. Lett.*, 1999, **82**, 4142–4145.
- 13 C. L. Evans and X. S. Xie, *Annu. Rev. Anal. Chem.*, 2008, **1**, 883–909.
- 14 R. Li, L. Wang, X. Mu, M. Chen and M. Sun, *J. Biophotonics*, 2019, **12**, e201900119.
- 15 L. Cui, R. Li, T. Mu, J. Wang, W. Zhang and M. Sun, *Spectrochim. Acta, Part A*, 2022, **264**, 120283.
- 16 S. Roy, P. J. Kinnius, R. P. Lucht and J. R. Gord, *Opt. Commun.*, 2008, **281**, 319–325.
- 17 Y. Song, H. Wu, G. Zhu, Y. Zeng, G. Yu and Y. Yang, *Combust. Flame*, 2022, **242**, 112166.
- 18 P. He, S. Li, R. Fan, Y. Xia, X. Yu, Y. Yao and D. Chen, *Opt. Commun.*, 2011, **284**, 4677–4682.
- 19 T. Kozai, S. Yamashita, K. Hirochi, H. Miyagawa, N. Tsurumachi, S. Koshihara, S. Nakanishi and H. Itoh, *Chem. Phys. Lett.*, 2012, **553**, 26–29.
- 20 R. Leonhardt, W. Holzappel, W. Zinth and W. Kaiser, *Chem. Phys. Lett.*, 1987, **133**, 373–377.
- 21 J. Faeder, I. Pinkas, G. Knopp, Y. Prior and D. J. Tannor, *J. Chem. Phys.*, 2001, **115**, 8440–8454.
- 22 A. Moradi-Araghi and M. Schwartz, *J. Chem. Phys.*, 1978, **68**, 5548–5552.
- 23 K. Tanabe and J. Hiraishi, *Adv. Mol. Relax. Interact. Processes*, 1980, **16**, 281–297.
- 24 W. G. Rothschild and R. M. Cavagnat, *J. Chem. Phys.*, 1992, **97**, 2900–2908.
- 25 D. J. Ulness, M. J. Stimson, J. C. Kirkwood and A. C. Albrecht, *J. Phys. Chem. A*, 1997, **101**, 4587–4591.
- 26 K. Tominaga and K. Yoshihara, *J. Phys. Chem. A*, 1998, **102**, 4222–4228.
- 27 Y.-H. Wang, Y.-J. Peng, X. He, Y.-F. Song and Y.-Q. Yang, *Chin. Phys. B*, 2009, **18**, 1463–1468.
- 28 M. J. Frisch, G. W. Trucks, H. B. Schlegel, G. E. Scuseria, M. A. Robb, J. R. Cheeseman, J. A. Montgomery, Jr., T. Vreven, K. N. Kudin, J. C. Burant, J. M. Millam, S. S. Iyengar, J. Tomasi, V. Barone, B. Mennucci, M. Cossi, G. Scalmani, N. Rega, G. A. Petersson, H. Nakatsuji, M. Hada, M. Ehara, K. Toyota, R. Fukuda, J. Hasegawa, M. Ishida, T. Nakajima, Y. Honda, O. Kitao, H. Nakai, M. Klene, X. Li, J. E. Knox, H. P. Hratchian, J. B. Cross, C. Adamo, J. Jaramillo, R. Gomperts, R. E. Stratmann, O. Yazyev, A. J. Austin, R. Cammi, C. Pomelli, J. W. Ochterski, P. Y. Ayala, K. Morokuma, G. A. Voth, P. Salvador, J. J. Dannenberg, V. G. Zakrzewski, S. Dapprich, A. D. Daniels, M. C. Strain, O. Farkas, D. K. Malick, A. D. Rabuck, K. Raghavachari, J. B. Foresman, J. V. Ortiz, Q. Cui, A. G. Baboul, S. Clifford, J. Cioslowski, B. B. Stefanov, G. Liu, A. Liashenko, P. Piskorz, I. Komaromi, R. L. Martin, D. J. Fox, T. Keith, M. A. Al-Laham, C. Y. Peng, A. Nanayakkara, M. Challacombe, P. M. W. Gill, B. Johnson, W. Chen, M. W. Wong, C. Gonzalez, and J. A. Pople, *Gaussian 03*, Gaussian, Inc., Wallingford CT, 2004, Vol. Revision E.01.
- 29 W. M. Dabodghao, *Indian J. Phys.*, 1930, **5**, 207–217.
- 30 A. Fendt, S. F. Fischer and W. Kaiser, *Chem. Phys.*, 1981, **57**, 55–64.
- 31 D. H. Rank and J. A. Van Horn, *J. Opt. Soc. Am. B*, 1946, **36**, 454–459.

